

FacePhys: State of the Heart Learning[♥]

Kegang Wang*
Tsinghua University

Jiankai Tang*
Tsinghua University

Yuntao Wang[†]
Tsinghua University

Xin Liu
University of Washington

Yuxuan Fan
Tsinghua University

Jiatong Ji
Tsinghua University

Yuanchun Shi
Tsinghua University

Daniel McDuff[†]
University of Washington

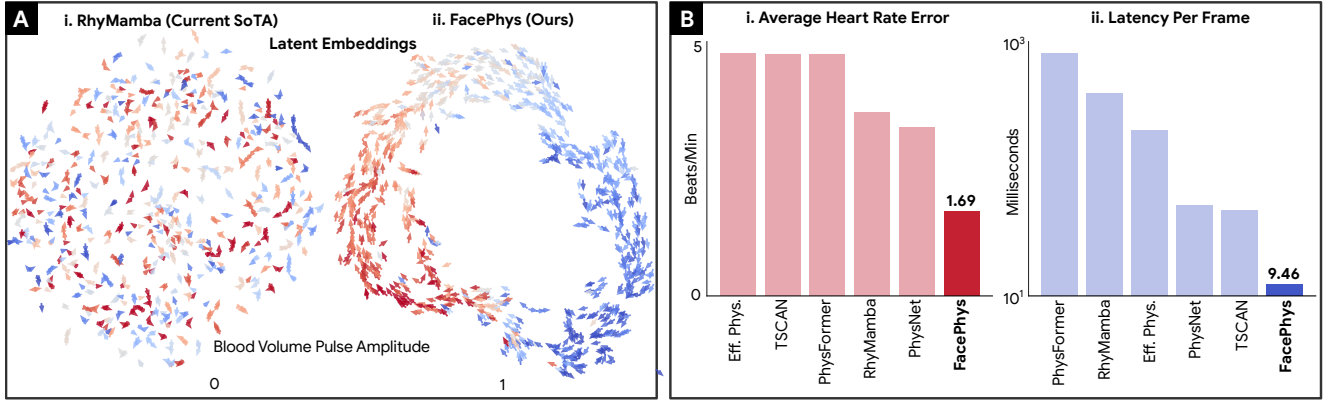


Figure 1. **The FacePhys State Space Model**, provides an effective representation of the cyclical nature of heart beats, as shown by the latent embeddings (A), combining high accuracy (B-i) and high efficiency (B-ii). We achieve gains of 49% in heart rate estimation and 83% in per-frame latency compared to the current state-of-the-art.

Abstract

Vital sign measurement using cameras presents opportunities for comfortable, ubiquitous health monitoring. Remote photoplethysmography (rPPG), a foundational technology, enables cardiac measurement through minute changes in light reflected from the skin. However, practical deployment is limited by the computational constraints of performing analysis on front-end devices and the accuracy degradation of transmitting data through compressive channels that reduce signal quality. We propose a memory efficient rPPG algorithm - FacePhys - built on temporal-spatial state space duality, which resolves the trilemma of model scalability, cross-dataset generalization, and real-time operation. Leveraging a transferable heart state, FacePhys captures subtle periodic variations across video frames while

maintaining a minimal computational overhead, enabling training on extended video sequences and supporting low-latency inference. FacePhys establishes a new state-of-the-art, with a substantial 49% reduction in error. Our solution enables real-time inference with a memory footprint of 3.6 MB and per-frame latency of 9.46 ms – surpassing existing methods by 83% to 99%. These results translate into reliable real-time performance in practical deployments, and a live demo is available at <https://www.facephys.com/>.

1. Introduction

Remote photoplethysmography (rPPG) is a non-contact technique for measuring cardiac activity by analyzing light reflected from skin [31]. The subtle pulsatile variations are typically not visible to the naked eye, but they can be captured by cameras and analyzed to recover heart rate [46],

* Co-first authors.

[†] Co-corresponding authors.

heart rate variability and other vital signs that can be derived from the waveform (e.g., blood pressure [5]). The attraction of non-invasive measurement of cardiac activity has led to rPPG technology being integrated into a number of applications, including health monitors [21, 28], emotion recognition systems [36, 44], and fatigue detection models [7].

Deep learning is the predominant and superior approach used in rPPG models [31], which can be effective at disentangling the cardiac pulse from head motions, ambient lighting changes, and other confounders [34, 38]. However, there are several reasons that performing inference *on-device* is very desirable, and this means high computational efficiency *and* accuracy are both important.

First, the PPG is degraded more than other information by video compression [32] meaning that it is optimal to process the video as close to the source as possible (i.e., on-device) rather than send it over a bandwidth limited network. **Second**, application of rPPG in resource limited settings, such as by mobile health workers in remote settings, means it many not be possible to rely on a cloud service. **Third**, cardiac measurement is a highly privacy sensitive application, with videos often containing a patient’s face and sensitive physiological signals. Further adding to why streaming and uploading to a server is not ideal. **Fourth**, the ability to run at a high frame rates enables opportunistic sensing (e.g., obtaining measurements each time you look at your phone) and helps capture waveform dynamics that could be used to detect arterial fibrillation [26] or hypertension [50] where high-frame rates (at least 100Hz) are a requirement to yield precise measurements. However rather leading to a decrease, the use of deep learning has meant that the computational resources required to run rPPG algorithms has *increased*, making practical applications and real-time inference challenging.

Some studies attempt to address efficiency issues by reducing the resolution of frames [2] or simplifying the model complexity [25]; however, these design choices invariably impact accuracy. Creating smaller, more memory efficient models [14, 20] often typically require slicing videos into shorter segments (e.g., 180 frames, approximately 6 seconds) [17, 27], an approach that overlooks the importance of longer-term temporal dependencies, leading to the loss of important information during training and inference, and making algorithms more susceptible to noise.

This paper proposes an accurate and memory-efficient rPPG model (**FacePhys**) built on neural Controlled Differential Equations (CDEs). FacePhys captures subtle spatial and temporal color changes corresponding to blood volume pulse, enabling accurate prediction of model states and the cardiac signal across arbitrarily long sequences. Leveraging temporal-spatial state space attention duality (TSD), FacePhys can be trained on sequences of frames and perform inference on a single frame, significantly reducing compu-

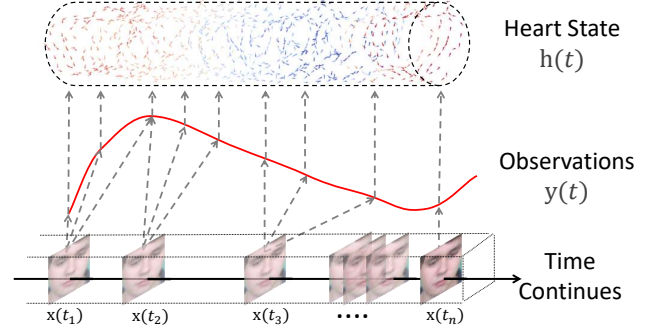


Figure 2. **The CDE form of the time-continuous heart state space** is used to describe the ideal heart state changes over time. However, it suffers from extremely low computational efficiency, its discretized form can be expressed as a state space model, with high computational efficiency.

tational load and achieving real-time inference. By learning a strong internal representation, FacePhys demonstrates superior performance across all datasets compared to state-of-the-art (SOTA) methods. The three core contributions of this paper are as follows:

1. We built FacePhys, a neural CDE-based heart state model with TSD that supports *single-frame* inference while preserving long-range periodic information.
2. We developed a discrete-time formulation that cuts the model memory footprint to **3.6 MB** (up to **98.4%** reduction) and achieves sub-**10 ms** inference latency (see Fig. 1), verified on real mobile browsers.
3. We evaluated FacePhys on large-scale datasets and demonstrated that it outperforms SOTA methods, including a **42.3%** improvement on the challenging MMPD dataset and up to **49%** overall improvement (Fig. 1B).

2. Related Work

Efficient rPPG Methods. The field of remote physiological sensing has evolved from handcrafted signal processing techniques, such as POS [45], to deep learning methods [9, 19]. Trained neural models have significantly improved accuracy and robustness. Early deep learning models in rPPG relied on CNN-based architectures, building on their success in other vision tasks. These methods extract features from facial video frames using convolutions and pooling, and then predict the rPPG signal using fully connected layers. Various types of CNNs, including 1D-CNN, 2D-CNN, and 3D-CNN, have been explored. Seq-rPPG [44] focuses on temporal features of facial videos using 1D-CNN, achieving stable performance with only an 8x8 facial region. DeepPhys [3] and TS-CAN [23] use 2D-CNNs to extract spatial features and introduce temporal shift modules for better heart rate estimation. PhysNet [51] and iBVPNet [15] employ 3D-

CNNs to extract spatio-temporal features, enhancing both accuracy and inference speed through attention mechanisms and lightweight networks. Despite their advancements, CNN-based models struggle to capture long-range dependencies, limiting their effectiveness in complex real-world scenarios [40]. Transformer-based methods address this limitation by leveraging self-attention mechanisms to extract features from the video frames. PhysFormer [53] is the first Transformer-based rPPG method, focusing on the temporal features of facial videos and achieving higher performance through long-range dependency self-attention mechanisms. RhythmFormer [54] proposes a hierarchical periodicity Transformer, achieving higher performance. Spiking-PhysFormer [22] proposes an rPPG method based on spiking neural networks, which achieves higher performance. Although Transformer methods have made significant progress in the rPPG field, their computational complexity makes them difficult to apply widely in practice. Approaches based on Mamba [29, 47, 49, 55] attempt to improve efficiency, but they remain difficult to run on embedded devices. Therefore, more efficient methods are needed to extract rPPG signals.

Neural Controlled Differential Equations (CDEs). Neural CDEs were proposed by Kidger et al. [16] as a generalization of neural ordinary differential equations (ODEs) that incorporates external input signals, with the aim of establishing a continuous-time hidden state dynamical system, thus enabling natural handling of time-continuous series. Theoretically, Neural CDE can be viewed as the limiting form of recurrent neural networks (RNNs) in the time-continuous scenario. Subsequent research has extended the applicability of neural CDE; for example, Neural RDE [33] discusses improving CDE to learn long sequences of physiological signals with noise, and Graph Neural RDE [4] generalizes it to spatiotemporal graph data.

State Space Models (SSMs). Early SSMs such as HiPPO [11] and S4 [12] model sequences via continuous-time ODEs, discretized for real-world data, achieving linear-time complexity compared to Transformers’ quadratic cost. Subsequent variants like S5 [35], H3 [8], Mamba [10], and Mamba-2 [6] enhance representational capacity and extend SSMs to vision tasks. Mamba introduces selective state updates for efficient long-sequence language modeling, while Mamba-2 unifies SSMs and transformers via a Structured State Space Duality (SSD) [6]. In vision, VideoMamba achieves state-of-the-art performance on long-term and high-resolution video understanding [18], and Mamba variants show broad success across image, point cloud, and multimodal applications [48]. These properties make SSMs promising for real-time video-based rPPG extraction.

Table 1. Computational Efficiency on CPUs

Method	Params	Mem.	Latency	FLOPs
EFFPhys	2,189	609	371	39.0
TSCAN	533	228	55.2	8.07
PhysNet	770	230	62.1	6.16
PhysFormer	7,395	576	2330	95.7
RhyMamba	4,936	347	889	27.4
FacePhys	719	3.6	9.46	0.15

Params (K) = Number of parameters. Mem (MB) = Memory usage. Latency (ms) = Inference time on CPUs. FLOPs (G) = Floating point operations.

3. Method

3.1. Basic Model

FacePhys extracts the heart state from continuous input $x(t)$, as shown in Fig. 2. The remote PPG signal $y(t)$ can be regarded as an observation of the heart state $h(t)$. The entire model can be written as a linear controlled differential equation (CDE), as in Equation (1).

$$\begin{aligned} h'(t) &= \mathbf{A}h(t) + \mathbf{B}x(t) \\ y(t) &= \mathbf{C}h(t) + \mathbf{D}x(t) \end{aligned} \quad (1)$$

where trainable \mathbf{A} is the state transition matrix, \mathbf{B} is the input matrix, \mathbf{C} is the output matrix, \mathbf{D} is the feedforward matrix, $x(t)$ is the control term (face information), $h(t)$ is the heart state, and $y(t)$ is the observation term (rPPG measurement).

We treat the underlying blood volume pulse as a latent dynamical system rather than a pure temporal dependency, and thus the state transition matrix encodes physiological periodicity instead of generic recurrence. As reported by PhysNet [51], the RNN variant underperforms its CNN counterpart; we therefore adopt CDEs as a continuous-time state-space formulation better aligned with physiological dynamics than discrete-time RNNs.

3.2. State Space Duality

Duality is a method for introducing efficient attention. Solving the CDE in Eq. (1) is very difficult and inefficient. This is because it describes a continuous-time state with an infinite sampling rate, while real videos consist of discrete frames. Inspired by Mamba-2 [6], we use a computationally efficient zero-order hold (ZOH) for discretization and introduce dual attention, yielding numerically stable and efficient SSM with strong periodic long-range temporal modeling while retaining the continuous-time inductive bias.

Using the ZOH discretization method, any Linear Time-Invariant (LTI) system can be discretized as follows: $\bar{A} = e^{\mathbf{A}\Delta t}$ and $\bar{B} = \left(\int_0^{\Delta t} e^{\mathbf{A}\tau} d\tau\right) \mathbf{B}$. This property ensures the equivalence of state transitions between the continuous and discrete systems, forming the core theorem of SSD.

The recursive relationship of the hidden state h_t is transformed into matrix multiplication via global convolution expansion: $h_t = \sum_{k=1}^t \bar{A}^{t-k} \bar{B} x_k$. By constraining matrix \bar{A} to be a diagonal matrix, matrix multiplication and inversion can be avoided. The global hidden state H , composed of hidden states from all time steps, is expressed as (2). Here, L is a lower triangular matrix, whose elements are defined as $L_{i,j} = \bar{A}^{i-j}$ when $i \geq j$, and \odot denotes the Hadamard product.

$$H = (L \odot (C\bar{B})) \cdot X \quad (2)$$

By making matrices C and \bar{B} dependent on the input, this formulation is equivalent to linear attention, expressed as $(L \odot (QK^T)) \cdot V$. Thus, SSD exhibits long-range modeling capabilities similar to those of transformers. Due to the step-by-step inference characteristics of SSMs, linear complexity can be achieved during inference as shown in Table 2, which enables efficient solving of the heart state CDE.

3.3. General Framework

Our framework is designed as a discretized CDE solver, which is a state space model with a structured dual form.

Due to the three-dimensional nature of video, we employ temporal-spatial decoupled modeling rather than a simple patch embedding. During training, it inputs video frames like a general rPPG model, outputs waveforms, and provides state transition results. It processes video sequence tensors $\mathbf{X} \in \mathbb{R}^{B \times T \times H \times W \times C}$ as input and extracts blood volume pulse (BVP) signals $\mathbf{y} \in \mathbb{R}^{B \times T}$ through temporal-spatial state space blocks. As illustrated in Figure 3, the computational workflow comprises two critical stages:

1. Temporal Normalization (TN): Independently performs detrending and standardization across the temporal dimension for each spatial coordinate.
2. Temporal-Spatial Modeling: Achieves periodic long-range temporal modeling through Temporal-Spatial SSM-Attention Duality (TSD).

Unlike traditional spatio-temporal joint modeling, TSD decouples spatial and temporal dimensions, utilizing 2D convolutions for spatial modeling while employing SSM duality for temporal modeling. This separation enables memory-efficient inference, achieved efficient attention with linear computational complexity. For a detailed comparison of memory efficiency with conventional architectures, refer to Table 2.

3.4. Temporal Normalization Module

The TN module [43] ensures the stability of temporal characteristics in long sequences. It begins by calculating the linear trend term using the least squares method, as formulated in Equation (3). During training, the trend estimation can be computed in parallel.

Table 2. **Memory Efficiency.** Comparison Between TSD and Traditional Structures.

Structure	Training Mem.	Inference Mem.
3D CNN	$O(Tk^3D)$	$O(k^3D)$
Transformer	$O(T^2D)$	$O(TD)$
TSD (Ours)	$O(TD)$	$O(D + L)$

L = SSD state dim. k = 3D kernel size. D = Feature dim. T = Time duration.

$$(\beta_0, \beta_1) = \arg \min_{\beta} \sum_{t=1}^T (x_t - (\beta_0 t + \beta_1))^2 \quad (3)$$

After obtaining the trend coefficients (β_0, β_1) , the residual of each pixel relative to the trend is computed and subsequently standardized as the final output.

$$\begin{cases} \text{Residual} & r_t = x_t - (\beta_0 t + \beta_1) \\ \text{S.D.} & \sigma = \sqrt{\frac{1}{T} \sum_{t=1}^T r_t^2} \\ \text{Output} & \tilde{x}_t = r_t / \sigma \end{cases}$$

To achieve constant time and space complexity during inference, the linear trend needs to be replaced with a Recursive Moving Average (RMA) trend.

$$\begin{cases} \text{RMA Trend} & \mu_t = \alpha \mu_{t-1} + (1 - \alpha) x_t \\ \text{Residual} & r_t = x_t - \mu_t \\ \text{S.D.} & \sigma_t = \sqrt{\alpha \sigma_{t-1}^2 + (1 - \alpha) r_t^2} \\ \text{Output} & \tilde{x}_t = r_t / \sigma_t \end{cases}$$

By updating the trend using RMA, there is no need to cache historical states, ensuring constant time and memory complexity. Moreover, RMA exhibits a strong similarity to the linear trend, making it an effective alternative for real-time processing.

3.5. Complex Diagonal State Transition Matrix A

$$h'(t) = \mathbf{A}h(t) + \mathbf{B}x(t) \quad (4)$$

The oscillatory term will introduce periodic representation, see Figure 4. The solution to the controlled ODE (4) consists of a homogeneous solution and a particular solution, where the particular solution depends on the control term, while the homogeneous solution describes the dissipation and oscillation components during state transition, which are determined by the eigenvalues of the trainable matrix \mathbf{A} . Since the control term $x(t)$ is governed by the input, we focus on the behavior of the homogeneous term. The cardiac pattern exhibits physiological periodicity, so matrix \mathbf{A} should include oscillatory terms. However, since

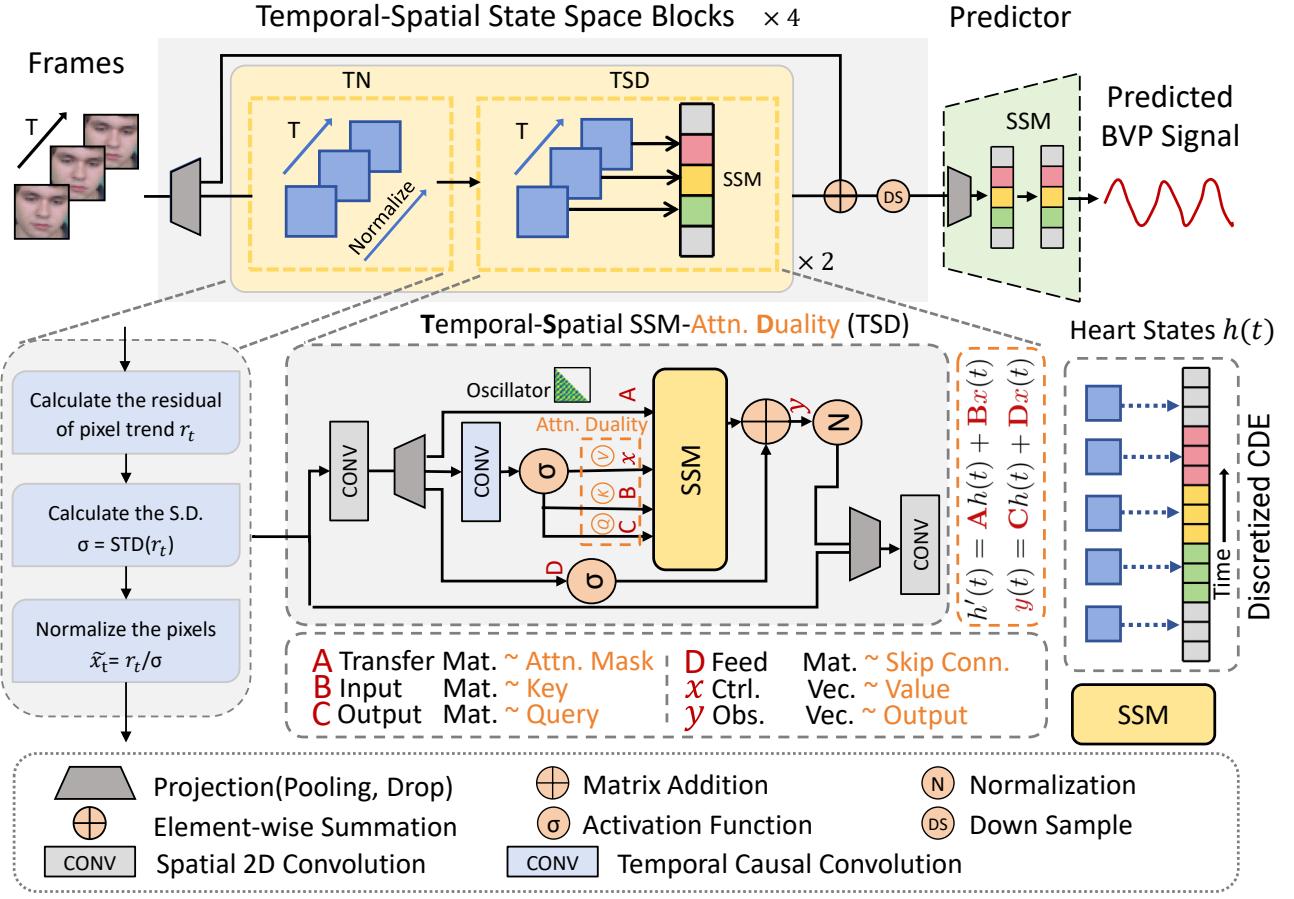


Figure 3. **FacePhys Framework.** Our framework utilizes the SSM dual as the core component, which serves both as an efficient discretization solver for the heart state CDE and as a linear attention processor. It employs Temporal Normalization (TN) to stabilize the extraction of temporal features and introduces a complex state transition matrix A to enable periodic attention.

Table 3. **Intra-Dataset Results.** FacePhys performed best across all datasets, when performing five-fold cross-validation.

Model	MMPD [38]			VitalVideo [41]			PURE [37]			UBFC [1]		
	MAE	RMSE	R	MAE	RMSE	R	MAE	RMSE	R	MAE	RMSE	R
EFFPhys [25]	14.8	20.3	0.31	2.35	7.17	0.83	1.63	3.12	0.98	3.41	6.55	0.89
TSCAN [24]	14.2	19.4	0.39	2.93	7.54	0.83	2.06	3.95	0.96	2.36	4.08	0.98
PhysNet [51]	8.13	12.4	0.56	0.69	2.66	0.98	0.93	2.08	0.99	1.76	2.92	0.98
PhysFormer [52]	9.47	14.0	0.47	0.66	2.76	0.98	2.66	5.32	0.90	5.42	8.99	0.85
RhyMamba [55]	8.21	12.0	0.61	0.83	3.69	0.96	0.26	0.53	1.00	0.53	0.73	1.00
FacePhys	5.58	10.2	0.72	0.64	2.66	0.98	0.26	0.53	1.00	0.46	0.67	1.00
Gains (%)	+31.4	+15.0	+18.0	+3.0	+0.0	+0.0	+0.0	+0.0	+0.0	+13.2	+8.2	+0.0

MAE \downarrow = Mean Absolute Error in HR estimation (Beats/Min). RMSE \downarrow = Root Mean Squared Error in HR estimation (Beats/Min). R \uparrow = Pearson Correlation in HR estimation.

S4D [13], many SSMs fix A to a real diagonal form for efficiency; this removes complex eigenvalues and suppresses oscillations (Eq. (5)). To match physiology without sacri-

ficing speed, we keep the trainable diagonal structure but allow complex diagonal entries, which restores oscillatory behavior.

Table 4. **Cross-dataset results.** FacePhys performs best in almost all comparisons when training on **RLAP**.

Model	MMPD [38]			VitalVideo [41]			PURE [37]			UBFC [1]		
	MAE	RMSE	R	MAE	RMSE	R	MAE	RMSE	R	MAE	RMSE	R
EFFPhys	9.18	13.7	0.56	6.75	19.3	0.51	2.48	5.48	0.98	0.81	1.71	1.00
TSCAN	10.2	15.2	0.47	4.20	8.86	0.78	3.90	7.05	0.96	0.90	1.66	1.00
PhysNet	11.2	16.4	0.42	0.89	3.56	0.96	0.63	2.34	1.00	0.66	1.03	1.00
PhysFormer	12.8	18.9	0.28	4.97	10.1	0.70	0.91	3.32	0.99	0.50	0.75	1.00
RhyMamba	9.62	14.9	0.47	2.85	8.91	0.80	1.63	4.55	0.98	0.44	0.68	1.00
FacePhys	5.30	10.0	0.76	0.77	3.07	0.97	0.24	0.68	1.00	0.43	0.67	1.00
Gains	+42.3	+27.0	+35.7	+13.5	+13.8	+1.0	+61.9	+70.9	+2.0	+2.3	+1.5	+0.0

MAE ↓ = Mean Absolute Error in HR estimation (Beats/Min). RMSE ↓ = Root Mean Squared Error in HR estimation (Beats/Min). R ↑ = Pearson Correlation in HR estimation.

Table 5. **Cross-dataset results.** FacePhys performs best in almost all comparisons when training on **PURE**.

Model	MMPD [38]			VitalVideo [41]			PURE [37]			UBFC [1]		
	MAE	RMSE	R	MAE	RMSE	R	MAE	RMSE	R	MAE	RMSE	R
EFFPhys	17.6	23.0	0.26	3.83	8.42	0.79	-	-	-	2.96	5.11	0.97
TSCAN	18.1	23.8	0.22	3.24	8.03	0.82	-	-	-	2.71	5.70	0.95
PhysNet	15.1	20.5	0.29	1.32	5.13	0.93	-	-	-	1.62	3.49	0.98
PhysFormer	13.0	18.1	0.44	1.08	4.07	0.95	-	-	-	1.15	2.06	0.99
RhyMamba	10.9	15.2	0.42	1.74	5.87	0.91	-	-	-	0.63	1.07	1.00
FacePhys	8.45	13.1	0.61	0.90	3.37	0.97	-	-	-	0.48	0.72	1.00
Gains	+22.5	+13.8	+38.6	+16.7	+17.2	+2.1				+23.8	+32.7	+0.0

MAE ↓ = Mean Absolute Error in HR estimation (Beats/Min). RMSE ↓ = Root Mean Squared Error in HR estimation (Beats/Min). R ↑ = Pearson Correlation in HR estimation.

$$h(t) = \sum_{j=1}^k c_j e^{\lambda_j t} v_j + \sum_{l=1}^m e^{\alpha_l t} [A_l \cos(\beta_l t) + B_l \sin(\beta_l t)] \quad (5)$$

Where: c_j are real constants (corresponding to real eigenvalues), A_l and B_l are real constant vectors (corresponding to pairs of complex eigenvalues), α_l and β_l are the real and imaginary parts of the complex eigenvalues. Clearly, a real diagonal matrix A has no complex eigenvalues and cannot produce periodic behavior. However, if we remove the diagonal constraint on A , the computational complexity increases from linear to $O(n^3)$, which cannot meet efficiency requirements. Therefore, introducing complex diagonal elements is considered to improve this. As shown in Eq. (2), the matrix L is equivalent to a causal mask, which describes the causality and decay behavior of state transitions. Its elements are determined by $L_{i,j} = \bar{A}^{i-j}$ when $i \geq j$, and the complex eigenvalues of A lead to periodic $L_{i,j}$, thus it is dual to a periodic attention mask.

4. Experiments

4.1. Datasets

We use five benchmark datasets to evaluate our method: UBFC-rPPG [1], PURE [37], MMPD [38], RLAP-rPPG [44], and VitalVideo [41]. UBFC-rPPG includes 43 RGB videos under controlled indoor lighting. PURE contains 59 videos with various head movements for motion robustness testing. MMPD comprises 660 videos under diverse lighting and activities. RLAP features 58 subjects with high synchronization. VitalVideo, the largest dataset, covers 893 subjects with varied skin tones and indoor lighting. These datasets were selected for accessibility, reliability, diversity, and synchronization quality, making them suitable for remote physiological signal extraction evaluation. All baselines are strictly reproduced according to the original papers and use the same training data and processing methods. FacePhys training details are provided in the supplementary material.

4.2. Comparison with State-of-the-Art Methods

Intra-dataset Experiments. We first compare our method with five SOTA methods (Efficient-Phys [25], TSCAN [24], PhysNet[51], PhysFormer [52], Rhythm-Mamba [55]) on four representative datasets (MMPD [38],

Table 6. **Training and Test Chunk Length Ablation.**
Longer video chunks leads to lower HR estimation error.

Train\Test	160	320	640	1280	1800
160	6.13	6.05	6.11	6.15	6.11
320	6.17	6.19	6.17	6.09	5.78
640	6.24	6.05	6.02	5.86	5.79
1280	5.92	5.91	5.80	5.66	5.75
1600	5.93	5.73	5.51	5.42	5.30

Experiments are trained on RLAP and tested on MMPD. MAE is calculated in HR estimation (Beats/Min). Each video is divided into chunks of different lengths.

VitalVideo [41], PURE [37], and UBFC [1]) using 5-fold subject-independent intra-dataset settings. The results are shown in Table 3. Our method outperforms all other methods on almost all datasets, demonstrating its effectiveness in remote PPG and HR estimation. Specifically, FacePhys achieves the lowest MAE of 5.58 on MMPD and the highest Pearson Correlation of 1.00 on PURE and UBFC datasets, highlighting its superior accuracy and reliability.

Cross-dataset Experiments. To assess the generalization ability of our method, we evaluate its performance in cross-dataset settings. The results in Tables 4 and 5 indicate that FacePhys achieves the best performance across *all* the cross-dataset settings, demonstrating strong generalization. Specifically, FacePhys achieves the lowest MAE of 5.30 and the highest R of 0.76 on the challenging MMPD dataset when trained on the RLAP dataset. FacePhys outperforms all methods on the largest VitalVideo dataset (MAE: 0.77, R: 0.97) when trained on either RLAP or PURE, confirming its robustness and reliability. Compared to cross-dataset results, FacePhys maintains consistent performance across different datasets, whereas other methods show significant performance drops and less consistent performance (i.e., the second best method for one setting is not consistently the second best). This demonstrates our method’s effectiveness in handling diverse real-world scenarios and generalizing well across datasets.

Computational Efficiency. We further assess the computational efficiency of our method by comparing its inference time against other SOTA approaches. As shown in Table 1, FacePhys achieves the best trade-off between accuracy and efficiency, underscoring its practicality for real-world applications. FacePhys achieves the lowest latency of 9.46 ms, which is even lower than the frame capture time of 33.3 ms at 30 fps, making it suitable for real-time PPG estimation on resource-constrained devices.

4.3. Ablation Studies

Ablation Study on Components. We conduct an ablation study to validate the effectiveness of each component in FacePhys. We compare the performance after removing different components, including TN, SSD modules and oscil-

lator matrix A. The results in Table 7 show that our method performs best when all components are included. The TN module maintains the stability of temporal features, while the SSD module provides attention to assign weights to different frames. After the trainable state transition matrix A is replaced with complex values, oscillatory term emerge, which enhances the model’s ability to represent periodicity.

Ablation Study on Training and Test Chunk Length.

We also examine the impact of different training and test chunk lengths on model performance. The results in Table 6 show that longer chunks lead to better performance by capturing more temporal information. This finding aligns with previous studies [55] that longer test lengths can improve rPPG performance. With our memory-efficient design, we can train on entire videos, further proving that longer training lengths also enhance performance. Our method achieves the best results with a training chunk length of 1600 and a test chunk length of 1800, demonstrating its effectiveness in handling long-term temporal dependencies.

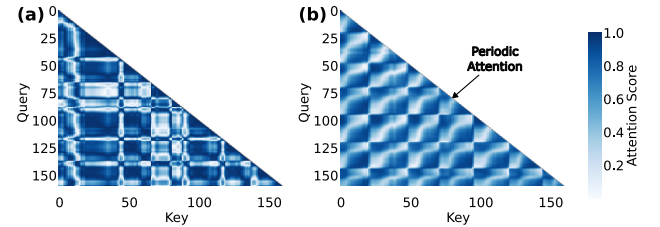


Figure 4. Introducing trainable complex numbers into the diagonalized state transition matrix A generates oscillatory terms in the solution, which is dual to periodic attention. (a) Original linear causal attention. (b) Periodic attention generated by FacePhys introducing complex numbers in A .

5. Discussion

5.1. An Effective and Generalizable Model

FacePhys exhibits state-of-the-art performance in intra-dataset and cross-dataset testing. The approach excels on MMPD and the large-scale VitalVideo dataset, both of which are the more challenging than PURE and UBFC (nearly saturated). In cross-dataset testing, FacePhys shows strong generalization, maintaining consistent performance, whereas other methods experience significant degradation. During cross-dataset validation, whether trained on RLAP or PURE, the MAE on VitalVideo and UBFC remains below 1 beat per minute. Additionally, on the MMPD dataset, which closely resembles real-world mobile scenarios, the lowest error achieved is 5.30 BPM, demonstrating its powerful performance on ubiquitous devices.

The robust generalization of FacePhys can be attributed to its TN and TSD architectural design. While our architecture inherits the computational efficiency of state-

Table 7. **Architecture Ablation.** Removing the Temporal Normalization, State Space or Oscillator Matrix A will harm performance.

Model	MMPD			VitalVideo			PURE			UBFC		
	MAE	RMSE	R	MAE	RMSE	R	MAE	RMSE	R	MAE	RMSE	R
w/o TN	11.6	17.6	0.43	0.88	3.45	0.97	0.80	3.97	0.99	0.52	0.73	1.00
w/o SSM Duality	10.8	16.7	0.51	1.10	3.80	0.96	0.34	0.87	1.00	0.63	0.85	1.00
w/o Oscillator	7.04	11.7	0.71	0.80	3.08	0.97	0.26	0.72	1.00	0.50	0.79	1.00
FacePhys	5.30	10.0	0.76	0.77	3.07	0.97	0.24	0.68	1.00	0.43	0.67	1.00
Gains	+24.5	+14.5	+7.0	+3.7	+0.3	+0.0	+7.7	+5.6	+0.0	+14.0	+8.2	+0.0

MAE ↓ = Mean Absolute Error in HR estimation (Beats/Min). RMSE ↓ = Root Mean Squared Error in HR estimation (Beats/Min). R ↑ = Pearson Correlation in HR estimation.

space modeling, it departs from prior Mamba-like works by embedding domain-specific physiological priors and 3D spatio-temporal coupling. Therefore, FacePhys should be viewed as a physiology-driven SSM. Studies [51] found that longer videos did not benefit CNN architectures due to limited receptive fields. As analyzed in Table 2, increasing the input length for Transformer architectures results in a quadratic increase in computational cost, which is impractical for large-scale training and inference. In contrast, FacePhys efficiently captures long-term dependencies with minimal computational overhead, allowing training on extended video segments and significantly enhancing cross-dataset generalization.

5.2. Efficient and Real-time FacePhys

Real-time performance is crucial for monitoring in medical and video streaming applications. Our user study indicates that the fluency and stability of rPPG systems significantly impact user experience and trust. Traditional methods like Green [42] use the average of the green channel of a single frame for rPPG prediction but suffer from motion artifacts. Subsequent deep learning methods improve performance but require long inputs, limiting real-time applications. While models like RT-rPPG [2] claim real-time inference, they still require pre-recorded input, preventing true streaming-based rPPG output. TS-CAN [23], which achieves a web application closest to our performance, requires users to record for 30 seconds before obtaining pulse waveform. With only 719K parameters, FacePhys uses 3.6 MB of memory and has a latency of 9.46 ms, making real-time rPPG prediction feasible on mobile devices. To the best of our knowledge, FacePhys is the first model to enable real-time rPPG waveform prediction while recording.

The real-time efficiency of FacePhys is mainly due to the transferable heart state space in our TSD architecture, updating frame-to-frame information rather than constructing dependencies within fixed video segments. This allows each frame to generate real-time BVP predictions and accumulate forward information for more stable predictions. The lightweight TN module and TSD design also contribute to FacePhys’s real-time performance, making it suitable for

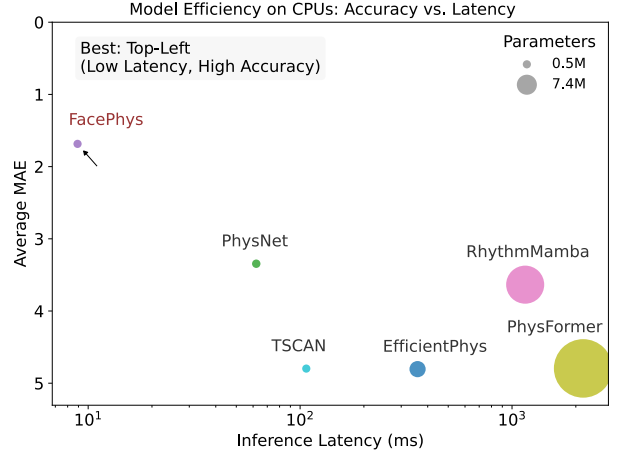


Figure 5. In terms of model accuracy and latency, through the heart state space model, FacePhys’s efficiency far exceeds that of previous methods.

time-sensitive and resource-limited applications.

5.3. Limitations and Future Work

Although FacePhys has made significant progress in performance and real-time capabilities, certain limitations remain. First, to ensure single frame inference, our model cannot access future information, this introduces lag. Second, although we validated our model on large scale diverse datasets, we have not yet tested it in hospital clinical scenarios, where performance for users with cardiovascular diseases remains to be evaluated.

Future work can extend FacePhys to predict additional cardiovascular signals from facial videos, including blood oxygen [39] and blood pressure [5]. Enhancing rPPG accuracy through multimodal fusion with thermal imaging or IMU sensors is another potential direction [30]. Optimizing computational efficiency will enable real-time processing at higher frame rates on lightweight hardware, expanding its practical applications in remote healthcare monitoring.

6. Conclusion

In this paper, we propose FacePhys, a memory-efficient rPPG algorithm based on temporal-spatial state space duality, designed for arbitrary length video training and inference. Our approach effectively captures subtle temporal changes and spatial representations of facial vascular information, achieving significant improvements over state-of-the-art methods on large-scale datasets such as MMPD and VitalVideo. FacePhys demonstrates superior accuracy and memory efficiency, with improvements of up to 60.3% in accuracy and 98.4% in memory efficiency. To the best of our knowledge, FacePhys is the first rPPG model capable of real-time inference from single-frame input, reducing computational load and achieving better user experience in real-world applications. Our method provides new directions for future research on rPPG, effectively balancing accuracy and efficiency for practical deployment.

References

- [1] Serge Bobbia, Richard Macwan, Yannick Benezeth, Alamin Mansouri, and Julien Dubois. Unsupervised skin tissue segmentation for remote photoplethysmography. *Pattern Recognition Letters*, 124:82–90, 2019. 5, 6, 7
- [2] Deivid Botina-Monsalve, Yannick Benezeth, and Johel Miteran. Rtrppg: An ultra light 3dcnn for real-time remote photoplethysmography. In *Proceedings of the IEEE/CVF Conference on Computer Vision and Pattern Recognition (CVPR) Workshops*, pages 2146–2154, 2022. 2, 8
- [3] Weixuan Chen and Daniel McDuff. Deepphys: Video-based physiological measurement using convolutional attention networks. In *Proceedings of the European Conference on Computer Vision (ECCV)*, pages 349–365, 2018. 2
- [4] Jeongwhan Choi and Noseong Park. Graph neural rough differential equations for traffic forecasting. *ACM Trans. Intell. Syst. Technol.*, 14(4), 2023. 3
- [5] Theodore Curran, Xin Liu, Daniel McDuff, Shwetak Patel, and Eugene Yang. Camera-based remote photoplethysmography to measure heart rate and blood pressure in ambulatory patients with cardiovascular disease: Preliminary analysis. *Journal of the American College of Cardiology*, 81 (8_Supplement):2301–2301, 2023. 2, 8
- [6] Tri Dao and Albert Gu. Transformers are SSMs: Generalized Models and Efficient Algorithms Through Structured State Space Duality. *ArXiv*, 2024. 3
- [7] Guanglong Du, Linlin Zhang, Kang Su, Xueqian Wang, Shaohua Teng, and Peter X. Liu. A Multimodal Fusion Fatigue Driving Detection Method Based on Heart Rate and PERCLOS. *IEEE Transactions on Intelligent Transportation Systems*, 23(11):21810–21820, 2022. 2
- [8] Daniel Y. Fu, Tri Dao, Khaled K. Saab, Armin W. Thomas, Atri Rudra, and Christopher Ré. Hungry hungry hippos: Towards language modeling with state space models, 2023. 3
- [9] John Gideon and Simon Stent. The way to my heart is through contrastive learning: Remote photoplethysmography from unlabelled video. *2021 IEEE/CVF International Conference on Computer Vision (ICCV)*, pages 3975–3984, 2021. 2
- [10] Albert Gu and Tri Dao. Mamba: Linear-Time Sequence Modeling with Selective State Spaces. *ArXiv*, 2023. 3
- [11] Albert Gu, Tri Dao, Stefano Ermon, Atri Rudra, and Christopher Re. Hippo: Recurrent memory with optimal polynomial projections, 2020. 3
- [12] Albert Gu, Karan Goel, and Christopher Ré. Efficiently modeling long sequences with structured state spaces, 2022. 3
- [13] Albert Gu, Ankit Gupta, Karan Goel, and Christopher Ré. On the parameterization and initialization of diagonal state space models, 2022. 5
- [14] Junfeng He, Khoi Pham, Nachiappan Valliappan, Pingmei Xu, Chase Roberts, Dmitry Lagun, and Vidhya Navalpakkam. On-device few-shot personalization for real-time gaze estimation. In *Proceedings of the IEEE International Conference on Computer Vision Workshops*, pages 0–0, 2019. 2
- [15] Jitesh Joshi and Youngjun Cho. Ibvp dataset: Rgb-thermal rppg dataset with high resolution signal quality labels. *Electronics*, 13(7):1334, 2024. 2
- [16] Patrick Kidger, James Morrill, James Foster, and Terry Lyons. Neural controlled differential equations for irregular time series. *Advances in neural information processing systems*, 33:6696–6707, 2020. 3
- [17] Hailan Kuang, Can Ao, Xiaolin Ma, and Xinhua Liu. Shuffle-rppgnet: Efficient network with global context for remote heart rate variability measurement. *IEEE Sensors Journal*, 2023. 2
- [18] Kunchang Li, Xinhao Li, Yi Wang, Yanan He, Yali Wang, Limin Wang, and Yu Qiao. VideoMamba: State Space Model for Efficient Video Understanding. *arXiv*, 2024. 3
- [19] Zhihua Li and Lijun Yin. Contactless pulse estimation leveraging pseudo labels and self-supervision. *2023 IEEE/CVF International Conference on Computer Vision (ICCV)*, pages 20531–20540, 2023. 2
- [20] Ji Lin, Chuang Gan, and Song Han. Tsm: Temporal shift module for efficient video understanding. In *Proceedings of the IEEE/CVF International Conference on Computer Vision*, pages 7083–7093, 2019. 2
- [21] Ke Liu, Jiankai Tang, Zhang Jiang, Yuntao Wang, Xiaojing Liu, Dong Li, and Yuanchun Shi. Summit vitals: Multi-camera and multi-signal biosensing at high altitudes. In *The 21st IEEE International Conference on Ubiquitous Intelligence and Computing (UIC 2024)*, 2024. 2
- [22] Mingxuan Liu, Jiankai Tang, Haoxiang Li, Jiahao Qi, Siwei Li, Kegang Wang, Yuntao Wang, and Hong Chen. Spiking-physformer: Camera-based remote photoplethysmography with parallel spike-driven transformer. *ArXiv*, abs/2402.04798, 2024. 3
- [23] Xin Liu, Josh Fromm, Shwetak Patel, and Daniel McDuff. Multi-task temporal shift attention networks for on-device contactless vitals measurement. *Advances in Neural Information Processing Systems*, 33:19400–19411, 2020. 2, 8
- [24] Xin Liu, Josh Fromm, Shwetak Patel, and Daniel McDuff. Multi-task temporal shift attention networks for on-device

- contactless vitals measurement. In *Advances in Neural Information Processing Systems*, pages 19400–19411. Curran Associates, Inc., 2020. 5, 6
- [25] Xin Liu, Brian L. Hill, Ziheng Jiang, Shwetak Patel, and Daniel McDuff. Efficientphys: Enabling simple, fast and accurate camera-based vitals measurement, 2021. 2, 5, 6
- [26] Xuenan Liu, Xuezhi Yang, Dingliang Wang, Alexander Wong, Likun Ma, and Longwei Li. VidAF: A Motion-Robust Model for Atrial Fibrillation Screening From Facial Videos. *IEEE Journal of Biomedical and Health Informatics*, 26(4): 1672–1683, 2022. 2
- [27] Xin Liu, Girish Narayanswamy, Akshay Paruchuri, Xiaoyu Zhang, Jiankai Tang, Yuzhe Zhang, Roni Sengupta, Shwetak Patel, Yuntao Wang, and Daniel McDuff. rppg-toolbox: Deep remote ppg toolbox. In *Advances in Neural Information Processing Systems*, pages 68485–68510. Curran Associates, Inc., 2023. 2
- [28] Hao Lu, Hu Han, and S Kevin Zhou. Dual-gan: Joint bvp and noise modeling for remote physiological measurement. In *Proceedings of the IEEE/CVF Conference on Computer Vision and Pattern Recognition*, pages 12404–12413, 2021. 2
- [29] Chaoqi Luo, Yiping Xie, and Zitong Yu. Phymamba: Efficient remote physiological measurement with slowfast temporal difference mamba. In *Chinese Conference on Biometric Recognition*, pages 248–259. Springer, 2024. 3
- [30] Xulin Ma*, Jiankai Tang*, Zhang Jiang, Songqin Cheng, Yuanchun Shi, Dong Li, Xin Liu, Daniel McDuff, Xiaojing Liu, and Yuntao Wang. Non-contact health monitoring during daily personal care routines. In *IEEE BSN 2025*, 2025. 8
- [31] Daniel McDuff. Camera measurement of physiological vital signs. *ACM Computing Surveys*, 55(9):1–40, 2023. 1, 2
- [32] Daniel McDuff, Ethan B. Blackford, and Justin R. Es-tepp. The impact of video compression on remote cardiac pulse measurement using imaging photoplethysmography. In *IEEE FG*, 2017. 2
- [33] James Morrill, Cristopher Salvi, Patrick Kidger, and James Foster. Neural rough differential equations for long time series. In *International Conference on Machine Learning*, pages 7829–7838. PMLR, 2021. 3
- [34] Ewa Nowara, Daniel McDuff, and Ashok Veeraraghavan. The Benefit of Distraction: Denoising Remote Vitals Measurements using Inverse Attention. *arXiv:2010.07770 [cs, eess]*, 2020. arXiv: 2010.07770. 2
- [35] Jimmy T. H. Smith, Andrew Warrington, and Scott W. Linderman. Simplified state space layers for sequence modeling, 2023. 3
- [36] Rencheng Song, Huan Chen, Juan Cheng, Chang Li, Yu Liu, and Xun Chen. PulseGAN: Learning to generate realistic pulse waveforms in remote photoplethysmography. *arXiv:2006.02699 [eess]*, 2020. arXiv: 2006.02699. 2
- [37] Ronny Stricker, Steffen Müller, and Horst-Michael Gross. Non-contact video-based pulse rate measurement on a mobile service robot. In *The 23rd IEEE International Symposium on Robot and Human Interactive Communication*, pages 1056–1062, 2014. 5, 6, 7
- [38] Jiankai Tang, Kequan Chen, Yuntao Wang, Yuanchun Shi, Shwetak Patel, Daniel McDuff, and Xin Liu. Mmpd: Multi-domain mobile video physiology dataset, 2023. 2, 5, 6
- [39] Jiankai Tang, Xin Liu, Daniel McDuff, Zhang Jiang, Hongming Hu, Luxi Zhou, Nodoka Nagao, Haruta Suzuki, Yuki Nagahama, Wei Li, et al. Camera measurement of blood oxygen saturation. *arXiv preprint arXiv:2503.01699*, 2025. 8
- [40] Jiankai Tang, Tao Zhang, Jia Li, Yiru Zhang, Mingyu Zhang, Kegang Wang, Yuming Hao, Bolin Wang, Haiyang Li, Xingyao Wang, et al. M3pd dataset: Dual-view photoplethysmography (ppg) using front-and-rear cameras of smartphones in lab and clinical settings. *arXiv preprint arXiv:2511.02349*, 2025. 3
- [41] Pieter-Jan Toye. Vital videos: A dataset of face videos with ppg and blood pressure ground truths. 2023. 5, 6, 7
- [42] Wim Verkruijsse, Lars O Svaasand, and J Stuart Nelson. Remote plethysmographic imaging using ambient light. *Optics express*, 16(26):21434–21445, 2008. 8
- [43] Kegang Wang, Jiankai Tang, Yantao Wei, Mingxuan Liu, Xin Liu, and Yuntao Wang. A plug-and-play temporal normalization module for robust remote photoplethysmography, 2024. 4
- [44] Kegang Wang, Yantao Wei, Jiankai Tang, Yuntao Wang, Mingwen Tong, Jie Gao, Yujian Ma, and Zhongjin Zhao. Camera-based hrv prediction for remote learning environments, 2024. 2, 6
- [45] Wenjin Wang, Albertus C. den Brinker, Sander Stuijk, and Gerard de Haan. Algorithmic principles of remote ppg. *IEEE Transactions on Biomedical Engineering*, 64(7):1479–1491, 2017. 2
- [46] Hao-Yu Wu, Michael Rubinstein, Eugene Shih, John Guttag, Frédo Durand, and William Freeman. Eulerian video magnification for revealing subtle changes in the world. *ACM transactions on graphics (TOG)*, 31(4):1–8, 2012. 1
- [47] Zheng Wu, Yiping Xie, Bo Zhao, Jiguang He, Fei Luo, Ning Deng, and Zitong Yu. Cardiacmamba: A multimodal rgb-rf fusion framework with state space models for remote physiological measurement. *arXiv preprint arXiv:2502.13624*, 2025. 3
- [48] Rui Xu, Shu Yang, Yihui Wang, Yu Cai, Bo Du, and Hao Chen. Visual Mamba: A Survey and New Outlooks, 2024. 3
- [49] Zhixin Yan, Yan Zhong, Hongbin Xu, Wenjun Zhang, Shangru Yi, Lin Shu, and Wenxiong Kang. Phymamba: State space duality model for remote physiological measurement. *arXiv preprint arXiv:2408.01077*, 2024. 3
- [50] Mototaka Yoshioka and Souksakhone Bounyong. Analysis of pulse transit time derived from imaging photoplethysmography and microwave sensor-based ballistocardiography. In *Proceedings of the IEEE/CVF Conference on Computer Vision and Pattern Recognition (CVPR) Workshops*, 2020. 2
- [51] Zitong Yu, Xiaobai Li, and Guoying Zhao. Remote photoplethysmograph signal measurement from facial videos using spatio-temporal networks. In *Proc. BMVC*, 2019. 2, 3, 5, 6, 8
- [52] Zitong Yu, Yuming Shen, Jingang Shi, Hengshuang Zhao, Philip Torr, and Guoying Zhao. Physformer: Facial video-

based physiological measurement with temporal difference transformer. In *CVPR*, 2022. [5](#), [6](#)

- [53] Zitong Yu, Yuming Shen, Jingang Shi, Hengshuang Zhao, Philip HS Torr, and Guoying Zhao. Physformer: Facial video-based physiological measurement with temporal difference transformer. In *Proceedings of the IEEE/CVF conference on computer vision and pattern recognition*, pages 4186–4196, 2022. [3](#)
- [54] Bochao Zou, Zizheng Guo, Jiansheng Chen, and Huimin Ma. Rhythmformer: Extracting rppg signals based on hierarchical temporal periodic transformer. *ArXiv*, abs/2402.12788, 2024. [3](#)
- [55] Bochao Zou, Zizheng Guo, Xiaocheng Hu, and Huimin Ma. Rhythmmamba: Fast, lightweight, and accurate remote physiological measurement. *Proceedings of the AAAI Conference on Artificial Intelligence*, 39(10):11077–11085, 2025. [3](#), [5](#), [6](#), [7](#)